The Effect of Nozzle Configuration on Local Convective Heat Transfer to Horizontal Plate Impinging Air Jet

Kalimuthu, Jeyajothi*+

Petrochemical Engineering, Mahendra Institute of Engineering and Technology, Namakkal- 637503, INDIA

M., Senthilkumar; S., Sadhishkumar; A., Jagadeesan

[4]Mechanical Engineering, Mahendra Institute of Engineering and Technology, Namakkal- 637503, INDIA

ABSTRACT: *In an impinging air jet, nozzle shape noticeably impacts heat transfer between jet and plate by affecting the velocity profile at the jet exit and thereby potentially modifying the behavior of the air jet vortex structures. This study analyzed the influence of four different injections (0 to 80 mm). They all possess the same free area and the equivalent diameter is D = 9 mm. Experiments have been conducted for Reynolds numbers 192.61< Re<1661.26, for orifice-to-plate distances 0.67 < H/D< 16, and for the temperature of the jet was conducted 115°C. In this effect which is greater in the round shaped orifice was taken. The velocity profile at the jet exit (6.4 and 9.2 m/s), for a distance from the point of impingement (x/D = 0 to 160) presents a shape for the round orifice (0.5 to 3 mm). Thermal results also show that a round orifice on higher heat transfer rate for injections. The measurements of parameters on the behavior of local heat transfer characteristic values on the impingement surface and the effect of the velocity values were discussed. From the results, it was observed that the peak of the heat transfer obtained at the impinging point higher jet velocity of 9.4m/s.*

KEYWORDS: *Orifice-to-plate spacing; Impinging jets; Reynolds numbers; Velocity profile; Plate impinging air jet.*

INTRODUCTION

Impinging jets are generally used to develop the rate of heat transfer between a fluid (air, water, mist, etc.) and a solid and are moderately employed to produce enhanced and thermal sight that has been studied in depth also with cooling or heating convection surface. Impinging jets are recognized as an efficient way to advance heat transfer mechanisms. They are broadly used in industry, mainly in manufacturing processes for cooling, heating, or drying materials. The influence of nozzle location and different shapes of heat transfer has been extensively studied in the literature on impinging jets. Moreover, attempts have been made to improve impingement heat transfer by changing the nozzle configuration, especially with regard to the velocity profile and turbulence levels at the nozzle exit. Taking into account the generation of vortices as well as ambient fluid entrainment, the flow structure produced by different nozzle geometries can be highly complex.

* *To whom correspondence should be addressed.*
+ E-mail: Corresponding author , jayaset@yahoo.com
1021-9986/2023/6/1938-1797 8/$/5.08

Many reviewers identified heat transfer rate was maximum at the stagnation point in heat transfer, distribution as regards tube or convergent injection. For low orifice-to-plate distances (H/D < 4), the heat transfer rate was actually minimum at the stagnation point and the primary peak was found to be r/D < 0.5 [1-4]. Investigated for heat transfer attributed this phenomenon to a significant increase in turbulence. It also studied the local velocity fluctuations by pointing out the interaction of shear layer vortices with the impingement plate [5-9]. Reported that the formation and appearance of the horseshoe vortices could be a periodic phenomenon, which occurs at a frequency similar to the cyclic vortices in the wake [10-13]. Some further observations of the horseshoe vortex, which formed around each impinging jet, were also observed with multiple jets in a cross-flow [14, 15]. Investigate mass transfer between a convergent nozzle and a plane circular orifice nozzle for a Reynolds number 1360 and jet-to-plate distances ranging from 1 to 5, observed that the mass transfer of an orifice impinging jet on a flat plate is 18% higher than is the case with a convergent nozzle jet [16]. Studied that the compared heat transfer between a chevron jet and circular jet with a range of jet-to-plate distances 2 < H/D < 10 and with a Reynolds number equal to 5000, concluded that heat transfer is improved with the chevron nozzle. In the center of the impinged area, the latter yields heat transfer values higher than those provided by the circular jet for all jet-to-plate distances [17]. Identification of flow regime with Reynolds number facilitates the creation of an ideal flow model for efficient fluid system design. Reynolds number is used in fluid mechanics to indicate whether the fluid flow past a body or in a duct is steady or turbulent. It depends upon the pressure, temperature, characteristic length, and mainstream velocity of an ideal gas [27-28].

Talebi et.al. investigated the forced convection of Cu and $Fe3O_4$ and Cu/Fe_3O_4 hybrid nanofluid in the laminar regime under constant heat flux conditions experimentally. Experiments are carried out in three volume fractions of 1, 2, 4 % and three Re numbers of 600, 1200, and 1800, and the local Nusselt number is measured. They found out the results showed that for nanofluid in simple and hybrid modes, with increasing the volume fraction of nanoparticles and Re number, the heat transfer coefficient is increased. Results revealed that the heat transfer rate is augmented for both cases of simple and hybrid nanofluids with a rise in the particle volume fractions or the Re number [29]. *Talebi et.al.* investigated the forced convection heat transfer of thermally developing Fe_2O_3/water nanoparticles inside a copper tube under a magnetic field created by a number of permanent flat magnets. Experiments have been carried out under a laminar flow regime and uniform heat flux boundary conditions and the influence of magnetic field position and intensity. The results showed that due to the influence of the magnetic field on the Fe_2O_3/water nanofluid, secondary flow, and boundary layer deformation occur, the heat transfer changes and its variation is dependent on the flow profile and intensity and position of the magnetic field [30].

Chamka et.al. investigated the transference of the hybrid nanofluids due to the natural propulsive like shrinkage and relaxation of the flexible walls and the motion has serious applications in several embryonic technologies. A mathematical model is suggested to explore the numerical simulation of the hybrid nanofluid flow inside a slant porous cavity to determine the impact of volume fraction, Rayleigh number, heat generation, and heat source length and location on magneto-free convective with entropy analysis. The outcomes indicate that the thermal performance reduces more in the case of high volume fraction in comparison with low concentration. The addition of nanoparticles for several Rayleigh numbers causes the thermal performance to decline [28].

The review of recent impinging jet research publications identified a series of engineering research tasks that are important for improving the design and resulting performance of impinging jets: (1) clearly resolve the physical mechanisms by which multiple peaks occur in the transfer coefficient profiles, and clarify which mechanism(s) dominate in various geometries and Reynolds number regimes, (2) develop a turbulence model, and associated wall treatment if necessary, that reliably and efficiently provides time-averaged transfer coefficients, (3) develop alternate nozzle and installation geometries that provide higher efficiency, meaning improved Nu profiles at either a set flow or set blower power, and (4) further explore the effects of jet interference in jet array geometries, both experimentally and numerically. This includes improved design of exit pathways for spent flow in array installations [31].

The calculation of heat transfer coefficients constitutes a crucial issue in the design and sizing of heat exchangers. The Wilson plot method and its modifications based on measured experimental data utilization provide an appropriate tool for the analysis of convection heat transfer

Table 1: Heated target plate material specification

Material	Specification	Dimension
Aluminium (AL)	Type 6082	150×150 ×3 mm3
	Tensile strength 130 MPa	
	Thermal conductivity 180 W/m K	
	Melting point 5550C	
	1% Mn, 1.2% Mg and 1.3% Si	
	Density 2700 kg/m3	

processes and the determination of convection coefficients in complex cases. A modification of the Wilson plot method for shell-and-tube condensers is proposed. The original Wilson plot method considers a constant value of thermal resistance on the condensation side. The heat transfer coefficient on the cooling side is determined based on the change in thermal resistance for different conditions (fluid velocity and temperature). The modification is based on the validation of the Nusselt theory for calculating the heat transfer coefficient on the condensation side. A change of thermal resistance on the condensation side is expected and the value is part of the calculation. It is possible to improve the determination accuracy of the criterion equation for the calculation of the heat transfer coefficient using the proposed modification. The criterion equation proposed by this modification for the tested shell-and-tube condenser achieves good agreement with the experimental results and also with commonly used theoretical methods [32].

In this paper, suggestions were given for comparing results from visualizations with wall pressure measurements and describing the test facilities and experimental conditions. After visualizations and measurements have been compared, a conclusion part is presented.

EXPERIMENTAL SETUP

The air jet from the nozzle impinges normally in the center of a heated target block. A representative picture of the air jet and nozzle element is shown in Fig. 1. The material of aluminium plates was used as a target surface. A Kapton heater (varivolt type 10-p capacity 10A) of placed at the back of the plate provides a uniform heating element (3950 W/m^2). The total power supplied is monitored using two digital multimeters one for the voltage and the other for the current. Temperatures at the center are measured using thermocouples inserted through holes machined through the thickness of the plate. The target plate and heater are inserted in an insulator/protractor assembly with the top surface of the target plate flushed with the surrounding top surfaces of the insulation. The insulated material used is firebrick (thermal conductivity 0.75 W/m k).

Experiments were carried out for different nozzle diameters at different heights by using an adjustable stand this was done at two airflow velocities. Heating and cooling of the target plate occur simultaneously. Usually, the steady state condition is considered to be achieved when the heat loss by convection from the top surface of the plate equals the heat conducted to the top surface of the heated plate. After attaining a steady state, the surface temperature of the plate was recorded. The heated target plate specification is listed in Table 1.

Velocity boundary layer

With the flow of a fluid over a flat plate, the velocity and the temperature of the fluid approaching the plate is uniform at U and T. The fluid can be considered as adjacent layers on top of each other. Assuming a no-slip condition at the wall, the velocity of the fluid layer at the wall is zero. The motionless layer slows down the particles of the neighboring fluid layers as a result of friction between the two adjacent layers. The presence of the plate is felt up to some distance from the plate beyond which the fluid velocity U remains unchanged. This region is called the velocity boundary layer **(***Schetz),* 1993].

Instrumentation for monitoring, controlling, and measuring

Instruments and gauges are divided into two categories according to their functional use. One set of instruments is used for monitoring and controlling the input parameters such as airflow, pressure, velocity, and heating element voltage/current/power as well as the nozzle height from the study plate surface. The other set of gadget's measures and indicates the temperature, an important factor determining the Nusselt number and thereby the heat transfer characteristics. The parameters being measured and the corresponding instruments are tabulated in Table 2. The schematic locations of the instruments in the experimental setup are highlighted in Fig. 1.

Uncertainty analysis

The uncertainties in the measured primary quantities and derived quantities are shown in Table 3. The proliferations of the error due to the uncertainties in the measured primary physical quantities are calculated using the method described by *Kline* and *McClintock,* (1953). The uncertainty in the values of the convective heat

Table 2: Input Variables Measuring Instrument

Parameter	Monitoring/ Controlling devices
Airflow volume	Rotameter
Air jet velocity	Digital anemometer
Air temperature	Analog mercury thermometer
Air pressure	Pressure gauge
Air flow regulator	Flow control valve
Heater power consumption	Digital multimeter
Heater power control	Rheostat to vary the resistance
Nozzle height	Calibrated variable stand
The temperature of the plate	The thermocouple of Cr - Al type

Table 3: Uncertainties in the Measured Primary Quantities and Derived Quantities

Quantities	Uncertainty
Heater input voltage (V)	±1.8%
Heater input current(I)	±1.8%
Air speed(v)	±0.5%
The temperature of the plate wall (T_w)	±0.75%
The temperature of the air (T_a)	±0.75%
Area of the plate(A)	±1.0%
Length or distance(L or D)	±0.5%
Heat flux (q)	±4.6%
Heat transfer coefficient (h)	±6.6%
Thermal conductivity(K)	±0.75%

Table 4: Input Parameters of Performance for Experiments

Input factors	Specification
Direct:	
Nozzle diameters (D)	0.5, 1.0, 1.5, 2.0, 2.5 and 3.0 mm
The geometric center height of nozzle (H)	2 mm
Temperature measuring distance (x) from impinging point	0, 22, 51 and 80 mm
The volume of airflow (v) to achieve the velocity of	6.4 and 9.2 m/s
The thickness of the plate (t)	2, 2.5 and 3 mm
Materials of plate	Aluminium
Derived:	
Velocity of air (v) by adjusting air flow volume	set at 6.4 and 9.2 m/s
Reynolds number (Re_D)	between 192.61 and 1661.26

transfer coefficient can be obtained from the combination of the listed uncertainties (Refer to Table 3). The value of the uncertainty in the flow-measuring device follows the data given by the manufacturer. The uncertainty in

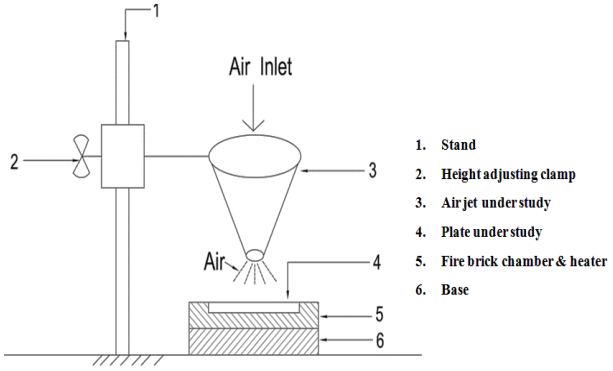

Fig.1: Representative picture of air jet and nozzle element

the measurement of the temperature is calculated by calibrating the thermocouple using a constant temperature. The equation for calculating the Nusselt Number with uncertainty could be written as,

$$Nu = \frac{(h \pm \varepsilon_h) \times (D \pm \varepsilon_D)}{(K \pm \varepsilon_K)} \quad (1)$$

Where ε is the relative uncertainty (%).

The Nusselt number uncertainties were carried out using the method of the uncertainty in Reynolds number was affected by the measurement of the flow rates and the nozzle exit area.

Therefore, by substituting the values from Table 3, the total uncertainty in the Nusselt number is 7.9%, which is below the permissible limit of less than 15% deviation [*Kline* and *McClintock*, 1953; *Kim et al*., 1993].

RESULTS AND DISCUSSIONS

The main account of the present study is on heat transfer characteristics on a local Nusselt number of a confined slot jet. A series of experiments invigilated are conducted to explore the flow and heat transfer characteristics in jet configuration. The input factors, both direct and derived ones and the experimental setup are the same for the entire study as tabulated in Table 4.

Effect of heights on Nu_L with various nozzle diameters and velocities

The experiments with various input factors, both direct and derived ones were carried out and the corresponding outcomes, namely the Local Nusselt number (Nu_L) were arrived at four different temperatures measuring locations using corresponding equations. Fig. 3. Compare the relationship between x and Nu_L with different nozzle diameters (D) at nozzle height of 2 mm, velocities of 6.4 and 9.2 m/s

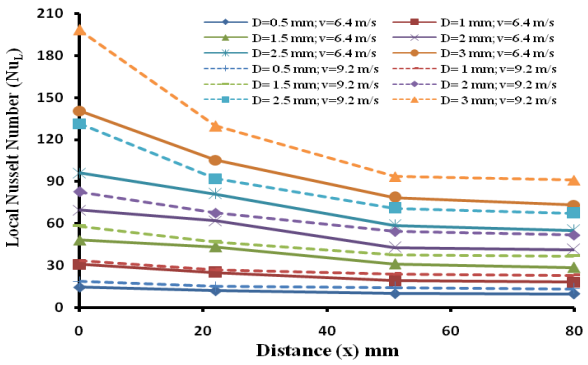

Fig. 2: Relationship between NuL with x at H = 2 mm; t = 2 mm and v = 6.4 and 9.2 m/s

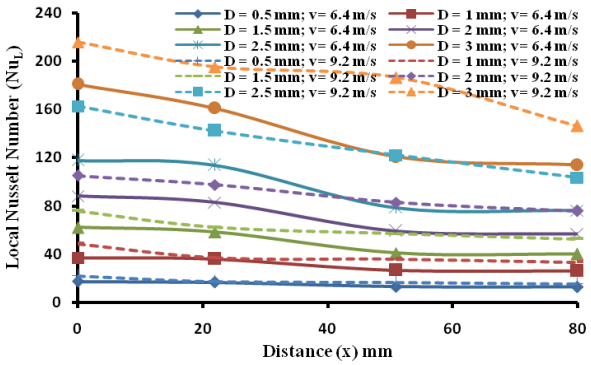

Fig.3: Relationship between NuL with x at H = 2 mm; t = 2.5 mm and v = 6.4 and 9.2 m/s

and plate thickness of 2 mm, 2.5 mm, 3 mm (Figs. 3, 4, 5 respectively).It is evident that the value of Nu_L increased with an increase in D and decreased as the distance from the point of impinging increased. This could be attributed to a strong downward flow from the stagnation region, which has retarded the flow transmission; which in turn has reduced the heat transfer.

Fig. 2 Represents 2 mm thickness plate for various nozzle diameters, different velocity profiles and a mixture of impingement distances in his graph. Analyzed that the local Nussult number maximum in the zero distance of the jet impingement at all the nozzle diameter and velocity was bigger than also maximize the Nusselt number. The range of irrespective diameter of all distances increases the Nusselt number from 0 to 22 mm moderately decreases and 22 mm to

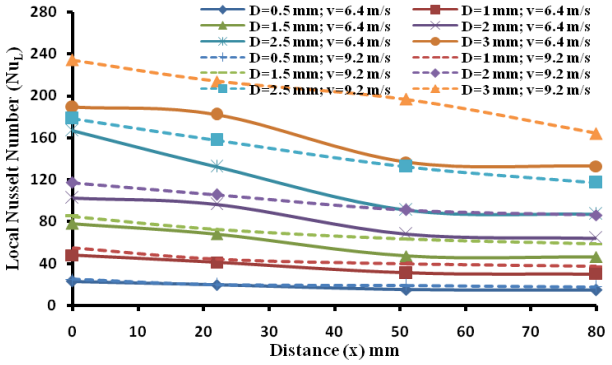

Fig.4: Relationship between NuL with x at H = 2 mm; t = 3 mm and v = 6.4 and 9.2 m/s

50 mm range is slightly moderate and finally 50 to 80 mm very few changes of decreasing the Nusselt number in the shown Figures. With the nozzle diameter D>1.5 mm, mostly reasonable changes for Nusselt number are easily identified in this particular air content more so, increase the Nusselt number compared to the other nozzle diameter.

Fig. 3 in this graph analysis for plate thickness 2.5 mm, nozzle diameter D < 0.5mm traceable Nusselt number rest of the D > 0.5 acknowledged easily in the chart. The maximum attained air content in this nozzle diameter of more than 2 mm to 3 mm increases in this Nusselt number, but decreases with distance wise can agree with this Fig.. In the distance of 20 to 80 mm, slightly more noticeable in these distances to cover. Compare the t= 2 mm plate better result in 2.5 mm at the maximum point achieved in that Nusselt number.

Fig. 4 shows that comparatively t= 2 and 3 mm more Nusselt number in the respective nozzle diameter in the varying thickness in this Fig. 3 mm plate thickness. In this graph trashing the distance increases the Nusselt number decreases to nozzle diameter less than 2 mm the more than 2 mm to 3mm evenly distributed the air content shown too identified. The traceable amount of changes in 60 mm to 80 mm distances irrespective of nozzle diameter, the bigger nozzle at a velocity higher range in this Figure. easily recognizes the chart and also a smaller velocity profile in the maximum nozzle diameter can observe be aware of in this Fig. 5.

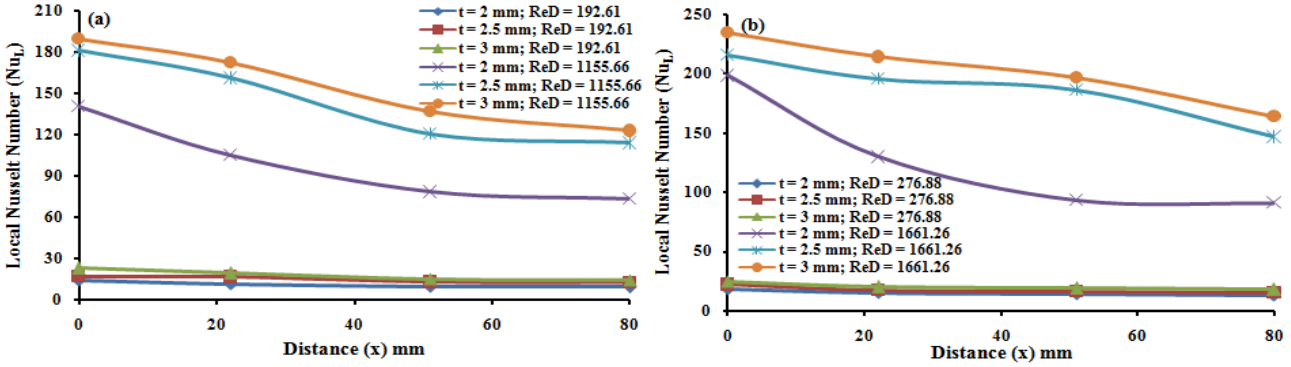

Fig.5 Relationship between Nu_L and x at D= 0.5 mm and 3 mm (Re_D=192.61, 1155.66) and (Re_D=276.88, 1661.26); t =2, 2.5, 3 mm; H= 2 mm at v=6.4 and 9.2 m/s (a, b).

In Fig. 5, the graph is shown between the local Nusselt number and distance at different velocities of 6.4 and 9.2 m/s hence, the local Nusselt number is decreased gradually from a distance at x = 0 to infinite distance in the Aluminium plates. At x = 0, the local Nusselt number is very high, so the heat transfer coefficient of air impingement on the surface of Aluminium plate. At x= 0 mm, the velocity profile is trending to be a laminar flow. But due to turbulence from x= 0 to x= 80 mm, the flow starts from laminar to turbulent. The velocity profile is very high on the surface layer. The fluid is restricted due to some momentum boundary layer beyond the thermal boundary layer by *Anwarullah et.al*., (2012) and *Lin et al*., (1997).

The effect of Re_D on Nu_L, the difference in Nu_L for different Re_D is noticeable at the impinging point, and the differences get reduced while moving away from the central point. The difference is quite significant at the impinging point for the higher Re_D compared to that of the lower Re_D. For the same Re_D, Nu_L increased with a decrease in H at the impinging point,and as x increases, only little variation in Nu_L is observed for all H. It can be observed that the graph of the lateral variation of the local Nusselt number becomes flattered and differentiation between the characteristic regions disappears similar to the previous studies.

From Fig. 5, at the initial stages, the drop is significant and tapered down at a later stage [Mahgoub, 2013]. The maximum Nu_L for higher velocity may be due to the fact that more quantity of air impinges on the target in the given time, which results in a higher rate of heat transfer by convection. Increasing the diameter of the nozzle also increased the efficiency of the forced convection, by increasing the area of impingement. Lesser nozzle height provides a concentrated jet with less dispersion, and the increased height reduces the force of the air jet.

CONCLUSIONS

The experimental runs were carried out for different values of nozzle diameter, flow velocity, and nozzle height. The heat transfer characteristics represented by the local Nusselt number are at the peak for the nozzle location, a height of 2.0 mm; for all the nozzles, although the actual values differ and distance of the impingement at maximum at zero point i.e stagnation zone. This tendency is followed for all the nozzles. The smaller nozzle of 6.4 m/s could have delivered a lower quantity of air compared to the of bigger nozzle of 9.2 m/s. This in turn has affected the stagnation Nusselt number and subsequently the heat transfer characteristics. This was mainly due to the reduction of airflow as the distance between the nozzle to the plate increased. This effect was witnessed because of higher airflow distribution. From the present study, it could be concluded that the peak of the heat transfer could be obtained at the impinging point higher jet velocity of 9.4m/s with a superior Reynolds number of 1661.26 for the biggest nozzle thickness of 3mm and the maximum Nusselt number was observed at 276.88.

Nomenclature

Nozzle Diameter	D
Orifice-to-plate distances	H/D
Distance from the point of impingement	x/D
Reynolds numbers	Re
Cromium – Aluminium	Cr - Al
Manganese, Magnesium and Silica	Mn,Mg,Si
Nessult Number	Nu

Local Nusselt number	Nu_L
thickness	t
Heater input voltage	V
Heater input current	I
Air speed	v
The temperature of the plate wall (Tw)	T_W
The temperature of the air	Ta
Area of the plate	A
Length or distance	L or D
Heat flux	q
Heat transfer coefficient	h
Thermal conductivity	K

Received : Jul.04, 2022 ; Accepted :Oct.24, 2022

REFERENCES

[1] Goldstein R., Behbahani A., Impingement of a Circular Jet with and without Cross Flow, *Int. J. Heat Mass Transfer*, **25**: 1377–1382 (1982).

[2] Baughn J., Shimizu S., Heat Transfer Measurements from a Surface with Uniform Heat Flux and an Impinging Jet, *ASME J. Heat Transfer*, **111**: 1096–1098 (1989).

[3] Fénot M., Vullierme J.-J., Dorignac E., Local Heat Transfer due to Several Configurations of Circular Air Jets Impinging on a Flat Plate with and without Semi-Confinement, *Int. J. Thermal Science*, **44**: 665–675 (2005).

[4] O'Donovan T.S., Murray D.B., Jet Impingement Heat Transfer – Part I: Mean and RMS Heat Transfer and Velocity Distributions, *Int. J. Heat Mass Transfer*, **50**: 3291–3301(2007).

[5] K.Jeyajothi and P. Kalaichelvi, Augmentation of Heat Transfer and Investigation of Fluid Flow Characteristics of an Impinging Air Jet on to a Flat Plat, *Arabian Journal for Science and Engineering*, 44 (2019), 6, pp. 5289-5299.

[6] Hoogendroorn C.J., The Effect of Turbulence on Heat Transfer at a Stagnation Point, *Int. J. Heat Mass Transfer*, **20:** 1333–1338 (1977).

[7] Lytle D., Webb B., Air Jet Impinging Heat Transfer at Low Nozzle-Plate Spacings, *Int. J. Heat Mass Transfer*, **37(12)**: 1687–1697 (1994).

[8] Colucci D.W., R. Viskanta, Effect of Nozzle Geometry on a Local Convective Heat Transfer to a Confined Impinging Air Jet, *Exp. Therm. Fluid Sci.*, **13**: 71–80 (1996).

[9] Krothapalli A., Lourenco L., Buchlin JM., Separated Flow Upstream of a Jet in a Cross-Flow, *AIAA J.* **28**: 414–420 (1990).

[10] Kelso RM., Smits AJ., Horseshoe Vortex Systems Resulting from the Interaction Between a Laminar Boundary Layer and a Transverse Jet, *Phys Fluids*, 7153–158 (1995).

[11] Jeyajothi K., Kalaichelvi P., Heat Transfer Performance of Stainless Steel, Mild Steel and Aluminium Target Plate for Various Configurations of Impinging Air Jet, *Bulgarian Chemical Communications*, **50(4)**: 631 – 637(2018).

[12] Andreopoulos J., Measurements in a Jet-Pipe Flow Issuing Perpendicularly into a Cross Stream, *J Fluids Eng*, **104**: 493–499. (1982).

[13] Barata J.M.M., Durao D.F.G., MV Heitor, Impingement of Single and Twin Turbulent Jets Through a Cross-Flow, *AIAA J.* **29**: 595–602(1991).

[14] Barata J.M.M., Fountain Flows Produced by Multiple Impinging Jets in a Cross-Flow, *AAIA J.*, **34**: 2523–2530(1996).

[15] Jeyajothi K., Kalaichelvi P., Effect of Steel Plate Thicknesses and Fluid Flow Characteristics of an Impinging Air Jet on Heat Transfer at Stagnation Point, *Brazilian Journal of Chemical Engineering*, **36(1)**: 221-228(2019).

[16] Amina M., Vaclav S., Florin B., Kodjovi S., Yassine Z., Ilinca N., Flow Dynamics and Mass Transfer in Impinging Circular Jet at Low Reynolds Number. Comparison of Convergent and Orifice Nozzles, *Int. J. Heat Mass Transfer*, **67**: 25–45(2013).

[17] Violato D., Laniro A., Cardone G., Scarano F., Three-Dimensional Vortex Dynamics and Convective Heat Transfer in Circular and Chevron Impinging Jets, *Int. J. Heat Fluid Flow*, **37**: 22–36(2012).

[18] Moffat R.J, Describing the Uncertainties in Experimental Results, *J. Fluid Sci.*, **1**: 3-17(1988).

[19] Schetz, Boundary Layer Analysis, *Prentice Hall, New Jersey*, (1993).

[20] Anwarullah M., Vasudeva Rao V., Sharma K.V., Effect of Nozzle Spacing on Heat Transfer and Fluid Flow Characteristics of an Impinging Circular Jet in Cooling of Electronic Components, *Int. J. Therm. Env. Eng.*, **4**: 7–12(2012).

[21] Kline S.J., McClintock F.A., Describing Uncertainties in Single Sample Experiments, *Mech. Eng.*, **75**: 3-8(1953).

[22] Lin Z.H., Chou Y.J., Hung Y.H., Heat Transfer Behaviours of a Confined Slot Jet Impingement, *Int. J. Heat Mass Transfer*, **40**: 1095–1107 (1997).

[23] Kim, J.H., Simon T. W., Viskanta R., Journal of Heat Transfer Policy on Reporting Uncertainties in Experimental Measurements and Results, *J. Heat Transfer*, **115**: 15–6(1993).

[24] Mahgoub, S.E., Forced Convection Heat Transfer Over a Flat plate in a Porous Medium, *Ain Shams Engineering Journal*, **4**: 605-613 (2013).

[25] Diop S.N., Biram D., Senaha I., A Study on Heat Transfer Characteristics by Impinging Jet with Several Velocities Distribution, *Case Studies in Thermal Engineering*, **26**: 101-111(2021).

[26] Cademartori S., Cravero C., Marini M., Marsano D., CFD Simulation of the Slot Jet Impingement Heat Transfer Process and Application to a Temperature Control System for Galvanizing Line of Metal Band, *Applied Sciences*, **11**: 1149 (2021).

[27] Bahmani A., Kargarsharifabad H., New Integral Solutions for Magnetohydrodynamic Free Convection of Power-Law Fluids Over a Horizontal Plate, *Iranian Journal of Science and Technology*, Transactions of Mechanical Engineering, (2019).

[28] Chamkha A.J., Armaghani T., Mansour M.A. , Rashad A.M., Kargarsharifabad H. , MHD Convection of an Al_2O_3–Cu/Water Hybrid Nanofluid in an Inclined Porous Cavity with Internal Heat Generation/Absorption, *Iranian Journal of Chemistry and Chemical Engineering (IJCCE)*, **41(3):** 936-956 (2022).

[29] Talebi M.H., Kalantar V., Nazari M.R., Kargarsharifabad H., Experimental Investigation of the Forced Convective Heat Transfer of hybrid Cu / Fe_3O_4 Nanofluids, *Journal of Solid and Fluid Mechanics*, **8**: 229-238 (2019).

[30] Talebi M.H., Kargarsharifabad H., Kalantar V., Nazari M.R., Experimental Study of the Effect of Position and Intensity of a Constant Magnetic Field on the Forced Convection Heat Transfer of Fe_2O_3 / Water Nanofluid in the Developing Thermal Region, *Journal of Solid and Fluid Mechanics*, **11**: 43-58(2021).

[31] Zuckerman N., Lior N., Jet Impingement Heat Transfer: Physics, Correlations, and Numerical Modeling, *Advances in Heat Transfer*, **39**: 565-631 (2006).

[32] Havlik J., Dlouhy T., Experimental Determination of the Heat Transfer Coefficient in Shell-and-Tube Condensers Using the Wilson Plot Method, *EPJ Web of Conferences*, **143**: 02035, (2017).